JOURNAL OF MATERIALS SCIENCE 39 (2004) 6421–6431

The role of the Al_2O_3 passivation shell surrounding nano-Al particles in the combustion synthesis of NiAl

J. J. GRANIER, K. B. PLANTIER, M. L. PANTOYA*
Mechanical Engineering Department, Texas Tech University, Lubbock, Texas 79409, USA
E-mail: michelle.pantoya@coe.ttu.edu

The self-propagating combustion behaviors of Nickel (Ni) and Aluminum (Al) thermites were studied as a function of bimodal Al particle size distributions. In particular, the low melting temperature of nano-scale Al particles coupled with the low concentrations of Al_2O_3 in micron-scale Al particles were exploited in order to optimize the macroscopic properties of the final alloy. Bimodal Al size distributions ranging from 0 to 50 wt% nano-Al combined with 50 wt% Ni were studied. Laser ignition experiments were performed on pressed pellets to determine flame propagation behavior and product microstructural features as a function of Al particle size. A new imaging technique is also presented that allows visualization of the surface reaction through highly luminescent flames and more accurate evaluation of burn rates. The wear behavior of the product alloy was measured and reported. Results show that composites composed of more micron-scale than nano-scale Al particles absorb more laser energy prior to flame propagation and experience an effective preheating. When 10–30 wt% nano Al is combined with micron Al and Ni, the wear resistance of the product alloy is optimized. Electron micrographs of the alloys suggest these properties may be attributed to whisker formations that behave as binding strings improving the overall abrasion resistance of the composite.

1. Introduction

Energetic composites consisting of sub-100 nanometer particle sizes offer the potential for advancements in powder metallurgy through the combustion synthesis of new alloys with improved macroscopic properties. The building blocks for these alloys are nano-scale particle reactants that consist of aluminum and another metal (i.e., nickel). In combustion synthesis, the metal matrix composite is ignited and the product alloy offers wear, thermal and/or corrosion resistance properties superior to other commercially available materials [1, 2]. These aluminum-based alloys (or aluminides) have applications in the aerospace and turbo-machinery industries.

Nano-scale aluminum is pyrophoric and must be stabilized for handling. An oxide passivation layer is 'grown' around core aluminum particles by controlling the pressure, temperature, and oxygen concentration exposure time to achieve a precisely controlled oxide layer thickness. This shell provides an air stable nano-aluminum particle. Campbell *et al*. [3] performed a molecular dynamic simulation on a 20 nm aluminum particle and showed that the oxide layer reached an equilibrium thickness of 3.3 nm after 260 picoseconds. These results are consistent with the 1–4 nm thick oxide shells that are typical of the nano-aluminum particles on the market today [4].

Because the surface area to volume ratio increases dramatically as particle diameter decreases, the oxide shell becomes a larger portion of the total material. Fig. 1 shows the variation in active aluminum content as a function of particle diameter for an oxide shell thickness ranging from 1–4 nm. These calculations were generated assuming spherical particles with a uniform oxide shell thickness. As particle size is reduced, the active aluminum content is decreased such that a trade-off may exist between the benefits of working on the nano-scale and the diminished purity of the Al particle.

Jones and coworkers [5, 6] studied the effect of the thickness of the passivation layer on the reactivity of Al nano-powders in air using thermal analysis techniques. Their results suggest that the thickness of the passivation layer does not significantly influence the reactivity of the material; but other factors play an important role such as, particle size distribution, degree of agglomeration and the composition of the passivation layer. Although the reactivity of the particle may not be strongly influenced by the thickness of the oxide shell, the increased Al_2O_3 content of nano-powders may

*Author to whom all correspondence should be addressed.

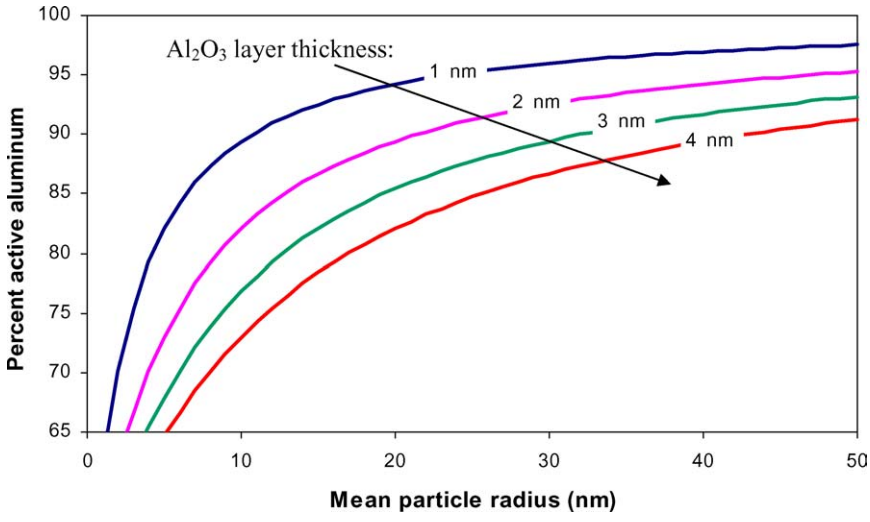

Figure 1 Active aluminum content as a function of particle radius for an oxide shell thickness of 1, 2, 3, and 4 nm.

significantly influence the microstructure and macroscopic properties of combustion synthesized alloys.

Granier and Pantoya [7] showed that nano-composite thermites are extremely sensitive to thermal ignition compared with traditional micron-composite thermites. In fact, they showed that ignition delay times were reduced by two orders of magnitude (from 10 s to 10 ms) using nano-scale rather than micron-scale Al particles [7]. They also showed significantly reduced ignition temperatures associated with nano-scale Al particles (i.e., 300 compared to 600°C) which is consistent with the reduced melting temperature of nano-scale Al particles [5].

Hunt *et al*. [8] studied the ignition and combustion behaviors of NiAl composed of nano-scale particles. They observed slower burn rates for nano-scale composites attributed to higher concentrations of Al_2O_3, which acts as a heat sink and retards flame propagation. Electron micrographs of the NiAl products reveal the formation of whiskers that are conjectured to be composed of Al_2O_3 in nano-scale composites but were not observed in micron-scale composites [8]. These fibrous hair-like structures may be linked to the higher percentage of Al_2O_3 that is present in the nano-scale Al composites.

Previous studies investigated adding particles of Al_2O_3 to the reactant matrix in an effort to improve the strength properties of the final material [2, 9]. Wang *et al*. [2] showed that the addition of inert diluents effectively reduces the combustion rate because the reactions produce less heat and there are longer transport distances between reactant. Lebrat *et al*. [9] found that adding greater than 10 wt% Al_2O_3 resulted in an incomplete reaction because the rate at which the Al liquid phase flows around the Ni particles is impeded by the presence of Al_2O_3 particles. An important factor in these previous studies is that the $Al_2O_3$was added in whisker or particle form. For the nano-scale particles considered in this study, the Al_2O_3 encapsulates each Al particle.

The objective of this study is to examine the effect of reducing particle size and increasing the Al_2O_3content on the macroscopic properties of NiAl product alloys. To examine the competing effects of particle size and Al_2O_3 concentration, a bi-modal size distribution for Al was prepared such that the nano-scale Al concentration varied from 0 to 100% of the total Al powder. Adding small amounts of nano-scale Al may promote increased sensitivity to ignition, as demonstrated in [7, 8] and may increase the wear properties of the final alloy, as suggested in [9]. To this end, requiring only small mass percentages of nano-scale particles may (1) reduce the material costs, because nano-scale particles can be expensive; (2) reduce the energy required for ignition, thereby increasing the efficiency of combustion synthesis and reducing the cost of an ignition source; and, (3) optimize the product alloy by enhancing the macroscopic properties.

2. Experimental procedures

Eleven powder mixtures were prepared with varying mass concentrations of nano and micron scale Al particles and sub-micron scale Ni particles. The nano-scale aluminum particles used in this study were produced using a gas condensation process, have an average particle diameter of 76 nm and purchased from Technanogy (Santa Ana, CA). The 12 μm Al and sub-micron Ni were both purchased from Sigma Aldrich (Milwaukee, WI). As the particle surface area to volume ratio increases, the 2.0 nm thick passivation layer surrounding the nano-Al particles becomes an appreciable component of the powder. Table I shows that the nano-scale Al consists of 19.6% Al_2O_3 while the micron-scale Al consists of only 1.5% Al_2O_3. In Table I, the average particle size is calculated from surface area measurements using a gas adsorption analyzer and Brauner Emmitt Teller (BET) theory. The oxide layer thickness is calculated

TABLE I Characterization of aluminum powders

Powder	Oxide shell thickness (nm)	% Al content	% Al_2O_3 content
76 nm Al	2.3	80.4	19.6
12 μm Al	2.0	98.5	1.5

TABLE II Mixture descriptions based on weight percent content of Ni, Al and Al_2O_3

Sample	A	B	C	D	E	F	G	H	I	J	K
Ni content (%)	50	50	50	50	50	50	50	50	50	50	50
Nano Al content (%)	0	5	10	15	20	25	30	35	40	45	50
nm-Al_2O_3 content (%)	0	0.98	1.96	2.94	3.92	4.9	5.88	6.86	7.84	8.82	9.8
Micron Al content (%)	50	45	40	35	30	25	20	15	10	5	0
μm-Al_2O_3 content (%)	1.0	0.9	0.8	0.7	0.6	0.5	0.4	0.3	0.2	0.1	0.0
Total Al (%)	49.0	48.1	47.2	46.4	45.5	44.6	43.7	42.8	42.0	41.1	40.2
Total Al_2O_3 (%)	1.0	1.9	2.8	3.6	4.5	5.4	6.3	7.2	7.2	8.9	9.8

from weight gain measurements using a Thermal Gravimetric Analyzer (TGA).

The powder mixtures were prepared such that a 50:50 weight concentration ratio of total Al to Ni was achieved. The 50-wt% Al consisted of a combination of the 76 nm and 12 μm particles that were varied by incrementally increasing the nano-Al particle content by 5 wt% and correspondingly decreasing the μm-Al particles by 5 wt%. In this way, the total amount of Al_2O_3 present in the mixture was controlled. Specifically, the Al_2O_3 content was incrementally increased from 1 wt% (with no nano-Al) to 9.8 wt% (with 50 wt% nano-Al). The eleven mixtures are described in more detail in Table II.

Each sample was mixed in solution using ultrasonic waves to break up agglomerates and improve the homogeneity of the final mixture. The solution was then evaporated away leaving a well-mixed powder sample that was pressure molded into pellets. A hardened steel plunger and 1018 steel barrel were used for the pressing process as shown in Fig. 2. The barrel was seated on the lower plunger ($L < 0.125$ in) allowing a loose seal with the inner diameter. A 500 mg powder sample was poured into the formed cup. The top plunger ($L = 1.5$ in) was aligned into the barrel tube and finally pressed to 8000 lbs or 40.7 kpsi corresponding to a 0.25-in diameter plunger. The bottom plunger was removed and the pellet extracted through the short length of the barrel tube. Three key points of the pressing process are: (1) the plunger material is much harder than the die barrel allowing the die and sample material to compress without deformation of the plunger; (2) a relatively loose tolerance (0.005-in) between the plunger and inner barrel wall to prevent galling and wedging such that the plunger could be extracted, cleaned and reused; and, (3) the bottom plunger is very short minimizing the extruding distance which can cause significant pellet deformation and cracking. With expected loss of powder sticking to the plunger and barrel walls, the final pressed sample has a 6.55 mm diameter, 4.25 mm length and 488–494 mg mass resulting in a 60% theoretical maximum density (TMD).

Six pellets were prepared for each of the eleven powder mixtures described in Table I. At 60% TMD the outer surface of the pellets have a highly reflective surface finish. For this reason, one of the flat surfaces was painted "flat black" with standard spray enamel to enable laser absorption and ignition of the reactants (Fig. 3A). The thickness of this paint layer is on the order of a micron and significantly smaller than the length of the pellet. Thus, the presence of the paint is not anticipated to alter the microstructure of the products or effect flame propagation through the pellet.

Two thermocouples were fixed inside and on the surface of the pellet. The first was a bare wire Type C thermocouple (0.005 in, Fig. 3B) inserted into a small hole drilled into the curved surface of the pellet and used to estimate flame temperature (Fig. 3A). A single bare wire Type S thermocouple (0.008 in) was set in spring tension against the front face of the pellet to estimate ignition temperature. Temperature data were recorded for both thermocouples at 9 kHz.

A 50-W CO_2 laser (10.6 μm wavelength) was used to ignite the black painted surface of each pellet. The

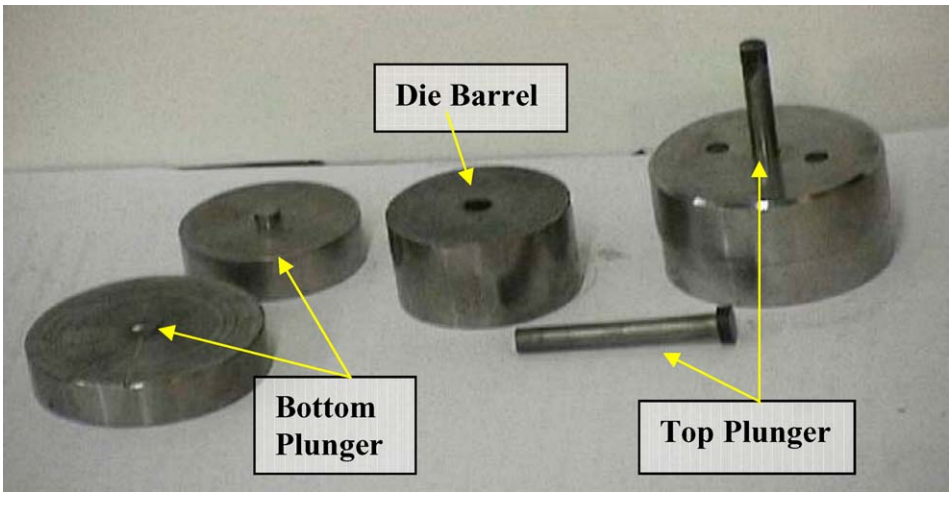

Figure 2 Photograph of the pressure molds for pellet pressing.

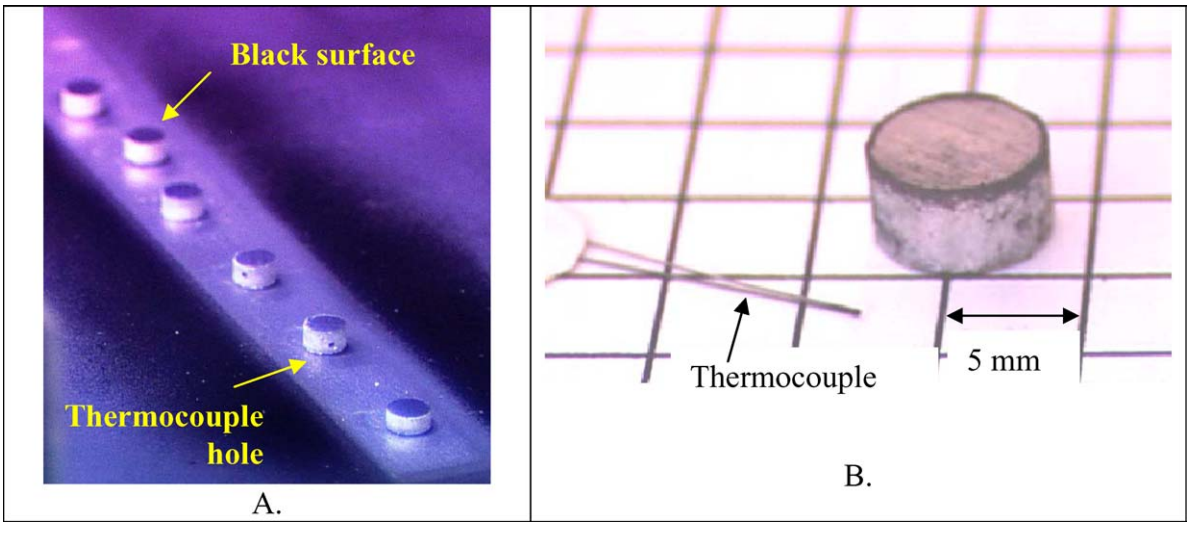

Figure 3 Photographs of the pellets. A. Illustrates black surface and thermocouple hole. B. Illustrates thermocouple and pellet.

beam was collimated to approximately a 6.5-mm waist with a 0.7 Gaussian fit (i.e., the intensity profile is similar to a typical flat top shape). The beam dynamics were characterized with a Pyrocam III Model PY-III-C-B beam profiler (courtesy of Spiricon Laser Beam Diagnostics, Logan, UT). A Phantom IV (Vision Research, Wayne, NJ) high-speed digital camera capable of capturing images up to 32,000 frames per second (fps) was oriented perpendicular to the laser beam and the curved surface of the pellet and used to analyze ignition and flame propagation.

Observations of thermite reactions indicate that they are highly luminescent. Coupling the high-speed camera with a copper vapor laser and using a notch filter on the camera lens effectively eliminates the intense illumination. In this way, the camera records reflected laser light from the reacting wave front. The idea works because the reflected laser light from the sample is significantly greater than the energy coming from the sample through the filter without laser illumination. This arrangement allows the camera to 'see' through flames and record details of processes that would otherwise be totally obscured by the background light. This method has proven to be ideal for eliminating image saturation and improving image quality. For each of the eleven powder mixtures two or three pellets were burned with the addition of the coupled copper vapor laser-high speed camera system. Multiple pellets from each series were also burned in an inert Argon environment and compared to those burned in an ambient air environment.

The copper vapor laser was integrated into the imaging diagnostics but may alter the evaluation of ignition time and flame propagation due to the added energy the laser imparts upon the reactants thereby effectively pre-heating the reactants. The copper vapor laser emits approximately 18 W at the fiber optic terminal and is rapidly diffused in 30° cone. The fiber optic terminal is placed about 1.5 inches away from the pellet to provide an appropriate level of green reflectance to the camera. This arrangement produces a laser flux contribution from the copper vapor laser of 0.01187 W/mm^2 to a half pellet surface area of 121 mm^2 resulting in approximately 1.5 W applied to the pellet for one to two seconds prior to CO_2 laser exposure. This small wattage may appear insignificant compared to the 50-W CO_2 laser ignition source but the thermocouples show that the laser flux from the copper vapor laser was enough to slightly elevate the initial temperature on the front surface and pellet center.

The products synthesized from this reaction were further analyzed for their bulk wear properties. Wear can be defined as damage to a solid surface, generally involving progressive loss of material, due to relative motion between that surface and another contacting substance [10]. The wear test was performed using a 3500 RPM belt sander with a 180 grit aluminum oxide belt. The product specimen was fixed to a confined location on the moving belt without applying a downward force. The mass of the sample was measured at two-minute intervals and the mass reduction due to abrasive wear was determined. The morphology of the product specimens was studied with a Hitachi S-570 SEM.

3. Results and discussion

Fig. 4A and B illustrate select still frame images captured from the high-speed camera without (Fig. 4A) and with the coupled copper vapor laser (CVL) (Fig. 4B). Both videos were recorded at 10,000 fps at a resolution of 64 × 128 pixels. A luminous flame front is obvious in sequence A while sequence B shows the reaction zone as a material transition from reactant to product shown by the change in surface finish and reflectivity. This imaging technique allows a new perspective on combustion processes in highly luminescent thermite reactions. From the data generated using the CVL—high-speed camera diagnostic technique, new estimates for burn rates can be measured that are based on clear observations of the reaction zone rather than measurements obscured by high intensity light.

Flame propagation in porous media can either appear quasi-homogeneous (i.e., planar) or scintillating based on flame spreading through the porous matrix. Mukasyan *et al.* [11] reported observing these two modes of flame propagation for various initial

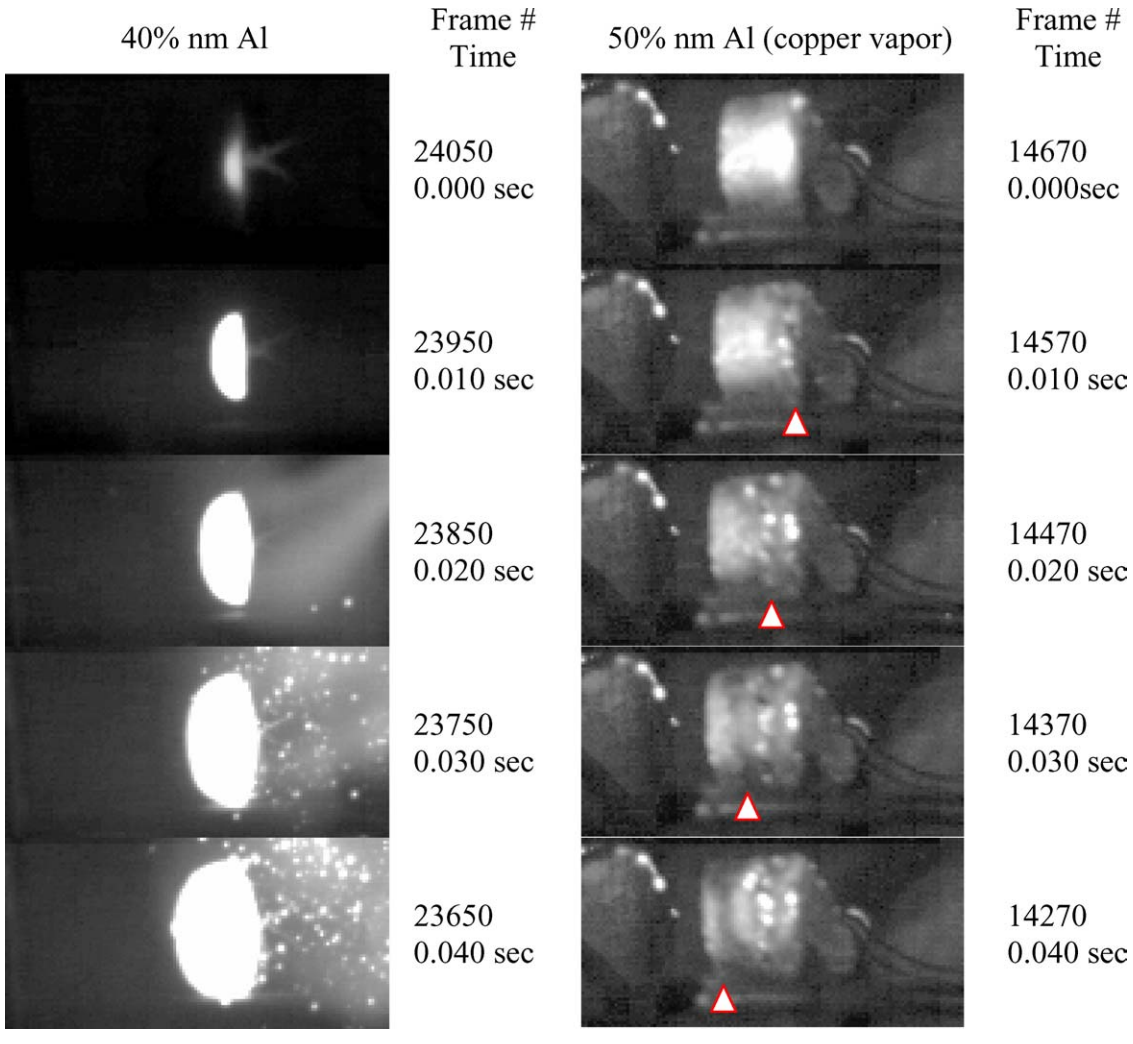

Figure 4 A series of still frame images captured 100 ms apart during flame propagation through A. Sample I (40% nano-Al, 10% micron-Al and 50% Ni) and without the copper vapor laser, B. Sample K (50% nano-Al and 50% Ni) and with the copper vapor laser. The reaction zone shown by material transition is indicated by Δ.

organizations of the reaction medium. For all cases in this study, the reaction zone appears to propagate through the sample in a planar, quasi-homogeneous fashion (Fig. 4B). Fig. 5 shows the burn rate measured by tracking the flame propagation as a function of time. Burn rates for samples with no nano-scale Al particles are significantly higher than those with nano-scale particles. Initially this behavior may appear counter-intuitive because smaller particles are typically associated with higher burn rates [12–15]. However, smaller particles contain significant levels of Al_2O_3 and retard flame propagation. The effect of Al_2O_3 can be seen by the reduced burn rates in Fig. 5 for even small amounts of Al_2O_3 (i.e., 1–2 wt%).

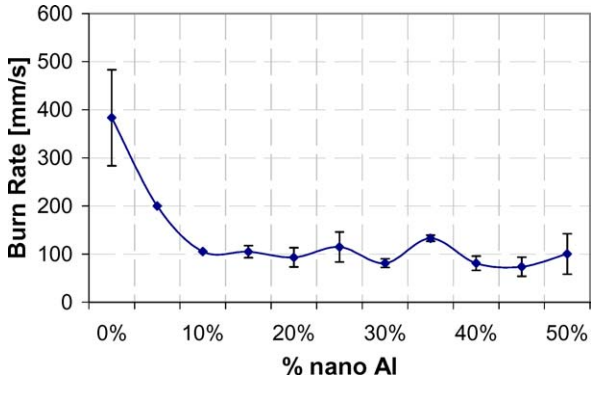

Figure 5 Burn rates for various samples listed according to wt% Nano-Al particles.

The mechanism controlling flame propagation may also influence the overall burn rate. For the fixed pellet densities studied here, the void spacing in Sample A (fully micron-Al particle composite) will be larger than the pellets containing nano-Al particles, even if the total amount of void space is the same (i.e., the bulk density of the pellets are equal). Larger void space may promote stronger convective mechanisms by providing open channels for flame spreading. Stronger convective mechanisms may contribute to the higher burn rates measured for Sample A.

Ignition and flame temperatures were recorded from the thermocouple data for five pellets in each sample set and the average and standard deviations are reported in Fig. 6. Curve A represents the ignition temperature measured at the front face of the pellet. Curve B shows the ignition temperature as a function of nano-Al particle content measured using the thermocouple inserted in the interior of the pellet. For all samples, the front face ignition temperature remains relatively constant at

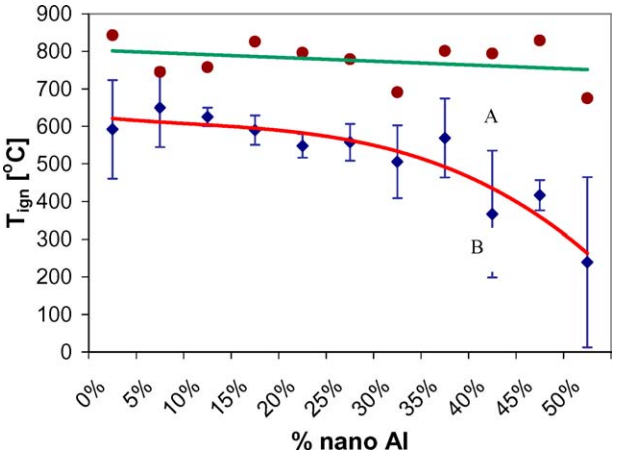

Figure 6 Ignition temperature as a function of nano-Al particle content. Curve A. Temperature was measured using S-type thermocouples located at front surface of the pellet. Curve B. Temperature was measured using C-type Thermocouples inserted in the interior of the pellet sample.

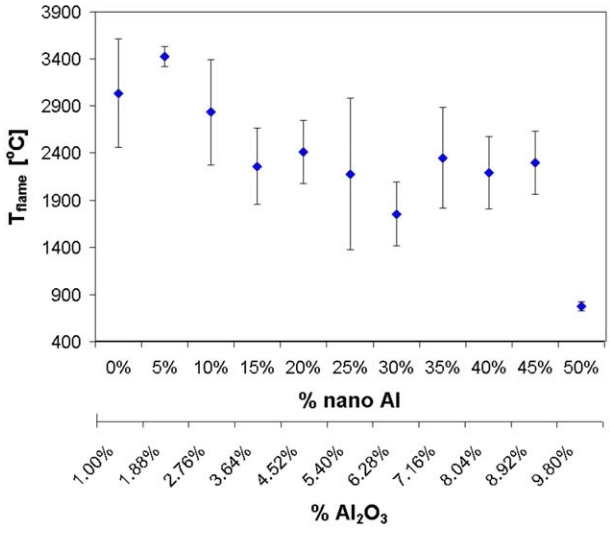

Figure 7 Measured peak temperatures (flame temperatures) as a function of percent nano-scale Al particles and Al_2O_3 content.

approximately 800°C but the pellet interior temperature (curve B) decreases with increasing nano-Al particle content. This behavior is consistent with earlier work that shows ignition temperatures are considerably lower for nano-Al based thermites than micron-Al based thermites [7]. Granier and Pantoya [7] suggest that this trend may result from the higher surface tension associated with nano-scale particles which manifests itself in the form of a depressed melting temperature for Al. Based on thermodynamic theory, the melting depression becomes noticeable at roughly 50 nm particle diameters [16]. Lower interior ignition temperatures for nano-Al based thermites may be partly attributed to the lower melting temperatures of nano-scale Al particles.

Thermites containing nano-Al particles are more sensitive to thermal stimuli and the reaction propagates at roughly ambient initial conditions (Fig. 6 curve B). Fig. 6 suggests that when the sample contains no nano-Al particles (i.e., Sample A), more energy must be stored within the pellet before the reaction is initiated and propagates. This is shown by the higher interior temperature associated with Sample A (Fig. 6 curve B). For example, the temperature difference between surface and interior for Sample A is roughly 200°C but is roughly 500°C for Sample K. This indicates that an increased level of energy is absorbed by the micron-composite such that the interior is pre-heated to a higher temperature prior to flame propagation. Reactions that propagate through reactants held at a higher initial temperature will burn at higher rates. This effective pre-heating behavior associated with samples containing little to no nano-Al particles may contribute to the higher burn rates measured in Fig. 5.

Fig. 7 shows measured flame temperatures from the thermocouple data. The samples containing no nano-scale Al particles (Sample A) burn at a much hotter temperature (3000°C) than the completely nano-Al samples (850°C) (Sample K). There may be multiple explanations for this behavior. When the larger micron-scale Al particles react, there is a larger volume of pure Al reactive with surrounding Ni elevating the reaction temperature. Also, Sample A is effectively preheated, exhibits higher burn rates and may also experience higher flame temperatures that result from the higher initial temperature conditions. Another possibility is that the nano-Al particles inherently contain a larger concentration of Al_2O_3 that will inhibit flame propagation. The increased concentration levels of Al_2O_3 may contribute to reduced measured flame temperatures.

Fig. 8 compares the SEM micrographs pre- and post-combustion for Sample B. Fig. 8A shows the Al and Ni particles segregated but packed in close proximity. In the product micrographs of Fig. 8B, the large μm Al spheres appear distinctly unreacted. The μm-scale Al particles may not be visible in the "before" images simply because during packing the submicron Ni and nm Al fill any void space between the larger spherical arc surface of the μm particles and the die walls. Fig. 8B clearly shows a 12-μm spherical Al particle with small whiskers or strands covering the surface (zoomed in on in the third image). The thin, needle-like whiskers are thought to be due to the cooling of vaporized Al_2O_3 [17, 18] and are not apparent prior to the reaction. The large μm mass is likely to be at a cooler temperature during the reaction such that the Al_2O_3 condenses on the surface forming whiskers. It is also interesting to note that the products behind the μm particles in Fig. 8B seem to be loosely joined meaning that even at the hotter temperatures not all of the μm particles reacted which may have altered the reaction and alloying of the surrounding sub-micron Ni and Al. The reactions studied here did not quench, however Fig. 8B implies that the reaction is incomplete. In all cases, the product matrix takes the same form as the reactant pellet.

Fig. 9A and B show the pre- and post-combustion images of Sample K (50 wt% nm Al). The reaction products appear to be in a more continuous state than Sample B from Fig. 8B. Even at the lower flame temperature of 850°C all of the nm Al particles appear to have reacted or at least the particles moved into a tighter joined matrix.

Fig. 10 is a magnified image of the highlighted top left corner of Fig. 9B. The whiskers in Fig. 8B are less than

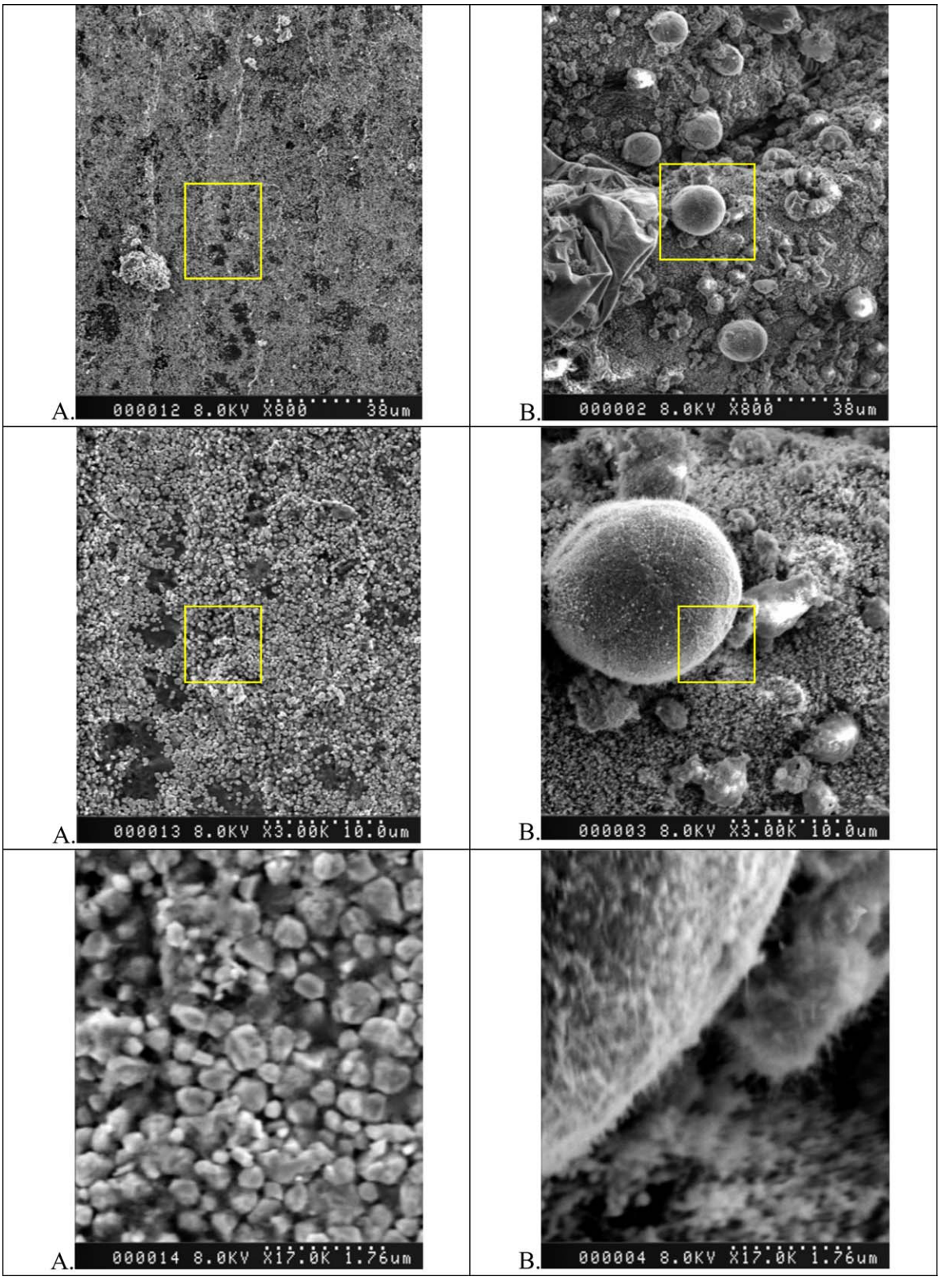

Figure 8 SEM micrographs of Sample B (5% nm Al with 45% μm Al). A. Pre-combustion (i.e., reactants); and, B. Post-combustion (i.e., products). Note the images are progressive enlargements of the square-highlighted regions.

1 μm in length and a magnified image of the whiskers in Fig. 9B show the whiskers are approximately 2 μm in length. This difference in size may be due to the reaction rate which controls how long the elevated temperature stays in a specific zone. Once the Al_2O_3 is formed, the rate of reverse sublimation or deposition (gas to solid) will control the crystal size. A slower deposition will allow the crystals to condense into a smaller whisker and a faster deposition will create longer whiskers in a weaker (less dense) crystalline structure.

The deposition interval can be defined as the time interval corresponding with the instant gaseous Al_2O_3 product is created to the instant the local temperature drops below the deposition temperature (i.e., melting

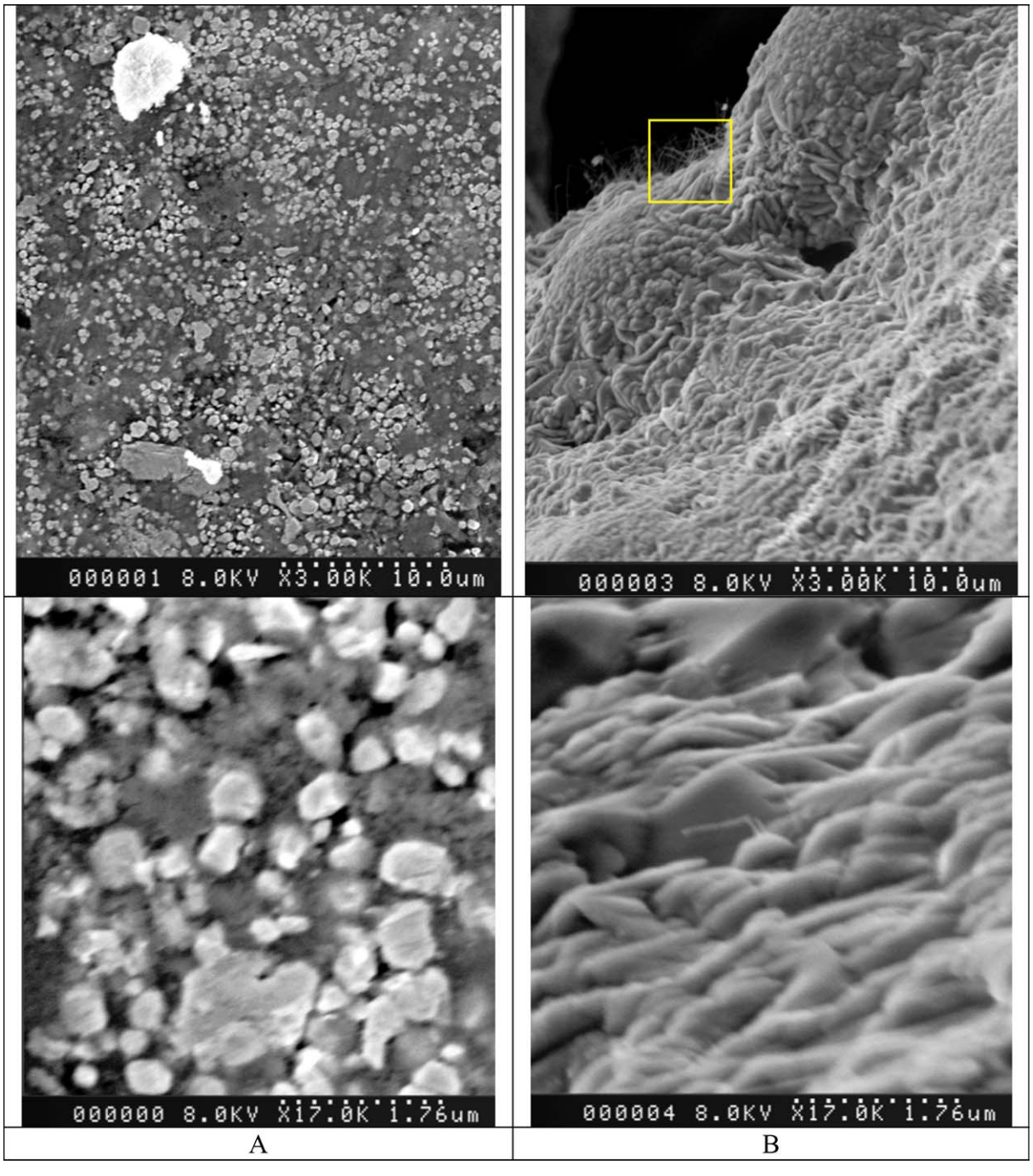

Figure 9 SEM micrographs of Sample K (50 wt% nano-scale Al) A. Pre-combustion (i.e., reactants); and, B. Post-combustion (i.e., products).

temperature of Al_2O_3 which is 2054°C) such that the crystalline solid Al_2O_3 completes formation. To justify the correlation between whisker lengths, deposition rate and deposition time interval, Fig. 11 shows a typical temperature history recorded by the surface and interior thermocouples for Samples A and E. From this figure, the deposition interval for Sample A is significantly longer than for samples containing nano-Al particles (Sample E). A longer deposition interval allows more time for a well-organized crystal growth resulting in a more compact lattice structure. This theory is consistent with the shorter whiskers associated with the 0 wt% nano-Al composites. The rapid solidification and crystal growth of nano-Al containing composites (Δt_{d1} from Fig. 11) results in less organized formation and a longer whisker.

Abrasion test results show that the intermediate bimodal mixtures display the highest abrasion resistance (Fig. 12). When the composite consists of 10 to 30 wt% nm Al particles, the product alloy exhibits improved tribological performance. When 10 wt% nano-Al powder is added to the reactant matrix, in spite of the poor interfacial interaction, the wear resistance of the matrix itself is improved by the presence of the few particles of nano-scale Al scattered throughout the matrix. As the amount of nano-scale powder is increased to 30 wt%, the wear is endured and the composite behaves almost as a granular structure, with little wear resistance. This may be attributed to the combined effects of an elevated flame temperature generated by the larger Al particles and the effective pre-heating of the reactants, and the low melt temperatures of the nano-scale Al particles

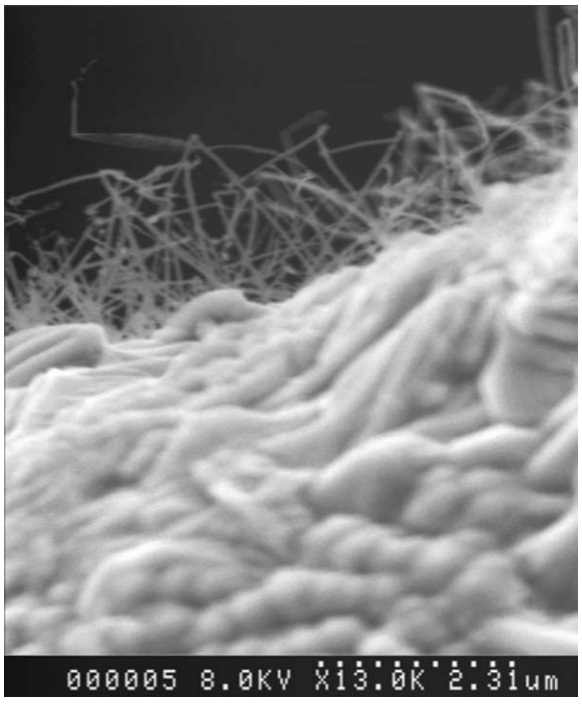

Figure 10 SEM close up micrograph of the highlighted region in Fig. 7B in which the whiskers can be more clearly seen.

which facilitate a complete reaction. These combined effects permit a combination of a relatively well-reacted alloy with enough Al_2O_3 to act as a strengthener without overpowering the combustion process. Also, the Al_2O_3 whiskers formed during the reaction may act as binding strings adding strength and wear resistance to the alloy. For the bimodal Al size distributions the whiskers are observed throughout the alloy matrix and mainly condense near the micron-scale Al particles.

These results have implications for volumetric rather than self-propagating combustion synthesis. For the high ignition powers used here, incomplete reactions are observed in the micrographs of some product samples (i.e., Samples A and B). The heating rate can be estimated as uT_{af}/δ, where u is the propagation velocity (Fig. 5, approximately 100 mm/s), T_{af} is the adiabatic flame temperature (Fig. 7, approximately 2500 K and δ is the reaction zone thickness (approximated as 0.5 mm from still frame images). The estimated heating rate is 500,000 K/s and the characteristic time for flame propagation across a 10-μm diameter Al particle is d/u and roughly 100 μs. The characteristic time for thermal diffusion through a 10-μm diameter Al particle can be estimated from the particle radius squared (5 μm) divided by the thermal diffusivity ($\sim 7 \times 10^{-5}$ m^2/s) and is roughly 4.0 μs. Therefore, a self-propagating flame travels faster than thermal diffusion through a micron scale particle and may contribute to the incomplete Al reaction observed in Fig. 8B. Essentially, the flame travels so fast that the micron scale particle may not fully respond (i.e., by complete melting) to the high temperature reaction wave. A slower and more controlled heating rate can result from volumetric combustion synthesis. The prolonged volumetric heating allows more time for a complete reaction between the micron-scale Al and Ni. Therefore, when working with micron-scale particles, the reaction may be encouraged to go towards completion if the reactants can be heated at lower rates, as in volumetric combustion synthesis. As reactant size approaches the nano-scale, higher heating rates associated with a self-propagating wave do not appear to result in incomplete reactions, as evidenced by Fig. 9. This may be attributed to (1) the higher surface area to volume ratio of the nano-scale particles which require less time to melt and react; and, (2) the lower melting temperature of nano-scale particles. For these reasons, the benefits of a self-propagating reaction may be realized in future studies that address nano-scale reactants.

When the concentration of the micron- or nano-scale Al particles is relatively high (below 5 and above

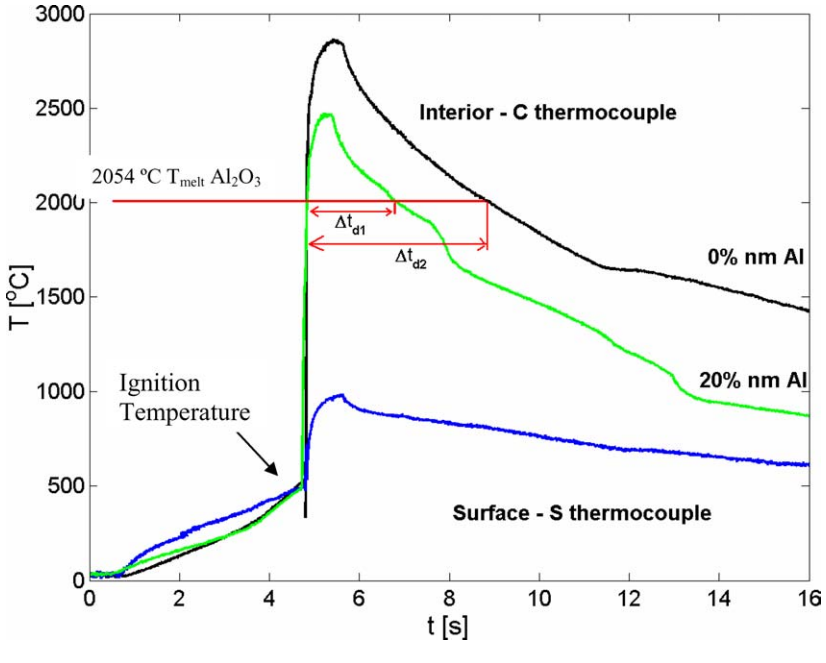

Figure 11 Temperature as a function of time for Sample A (0 wt% nano-Al) and Sample E (20 wt% nano-Al), measured from thermocouples located at the interior and surface of the pellet.

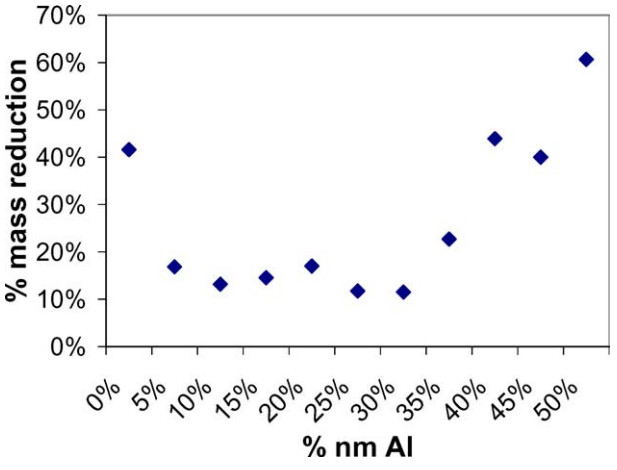

Figure 12 Abrasion testing for Samples A-K reported in terms of percent mass reduction.

30 wt% nano-particles, respectively), the wear endurance of the material decreases (Fig. 12). Higher concentrations of nano-Al particles add increased levels of Al_2O_3 such that the reaction temperature is lowered. Also, whisker formation resulting from condensed vapor phase Al_2O_3 is limited to the outside surface of the pellet. Therefore the binding strings that may strengthen the bimodal composites are only formed near the edges of the pellet and not throughout the alloy matrix. This results from a lack of 'cooler' micron-scale Al particles within the interior of the pellet that provide a relatively cold spot for the Al_2O_3 to condense and form. When no micron-Al is present, the whiskers are limited to the outer portion of the pellet where Al_2O_3 can condense in the presence of cooler air, as observed in Fig. 9. Without the binding whiskers throughout the matrix, the tribology of the alloy is reduced. Conversely, very low concentrations of nano-scale Al particles (0–5 wt%) result in an incomplete reaction such that the product alloy acts as a two phase system: un-reacted Al and product phases, as observed in Fig. 8. The result is a poor non-uniform microstructure with little abrasion resistance.

4. Conclusions

Bimodal size distributions ranging from nano- to micron-scale aluminum were prepared and combined with nickel. Self-propagating reactions were observed using a new imaging technique that allows observation of a reaction by peering through highly luminescent flames. The imaging technique utilizes a copper vapor laser coupled with a high-speed camera and a notch filter. The system eliminates the broadband light emitted by the reacting thermite and focuses only of the scattered laser light interacting with the combusting sample. In this arrangement, burn rates were measured as a material transition based on reflected laser light rather than tracing a highly luminescent flame profile. This technique offers a new perspective on flame propagation and allows measurement of burn rates.

The burn rates were found to decrease from 400 to 100 mm/s with the addition of even small amounts of nano-scale Al (i.e., 5 wt%). Ignition temperatures are roughly the same (800°C) for all samples, but interior temperatures indicate that there is substantially more energy absorbed by the little to no nano-Al containing composites such that these samples are effectively preheated prior to flame propagation. These increased initial temperature conditions may contribute to the higher burn rates associated with the micron-Al composites. It is also noted that the addition of nano-scale Al is accompanied by increased concentrations of Al_2O_3. Lower flame temperatures were measured for increased levels of Al_2O_3 (increased nano-Al content) and the fully nano-scale Al particle composites were observed to react to completion.

Whisker formation was observed in all samples containing nano-scale Al particles. The whiskers are conjectured to be composed of Al_2O_3 that vaporizes during the reaction and condenses as crystalline fiber-like structures. These whiskers are observed to form on or near micron-scale Al particles or for the fully nano-scale Al composite, on the outer perimeter of the pellet. The whiskers are thought to behave as binding strings and promote increased wear properties.

Abrasion tests on all product alloys reveal that 10–30 wt% nano-scale Al particle composites provides optimum wear properties. This result suggests that a combination of the properties inherent in micron and nano-scale Al particles optimize the bulk wear properties of the product alloy. For example, elevated flame temperature generated by the presence of larger Al particles and the effective pre-heating of the reactants coupled with the low melt temperatures of the nano-scale Al particles facilitate a complete reaction with improved wear characteristics. These combined effects permit a combination of a relatively well-reacted alloy with enough Al_2O_3 to act as a strengthener without overpowering the combustion process.

Incorporating nano-scale Al particles was also shown to promote a more complete reaction at high reaction rates. Results from this study suggest that Al-based alloys previously formed by volumetric combustion synthesis can now be synthesized using self propagating high temperature synthesis (SHS) because nano particles melt at lower temperatures than the bulk such that complete reactions are encouraged. This finding may permit the combustion synthesis of alloys previously unattainable through SHS techniques.

Acknowledgements

The authors gratefully acknowledge the support of the National Science Foundation under grant number CTS-0210141 and our program manager, Dr. Farley Fisher. The authors are also thankful for support provided by the Army Research Office under grant number DAAD19-02-1-0214 and our ARO program manager, Dr. David Mann. Dr. Mark Grimson (TTU) is acknowledged for his valuable expertise regarding SEM imaging.

References

1. A. VARMA, *Scientific American*, Aug. (2000) 58.
2. L. L. WANG, Z. A. MUNIR and Y. M. MAXIMOV, *J. Mater. Sci.* (1993).

3. T. CAMPBELL, R. K. KALIA, A. NAKANO, P. VASHISHTA, S. OGATA and S. ROGERS, *Phys. Rev. Lett.*, **82**(24) (1999) 4866.
4. "Personal Communication with Technanogy, Inc." (Santa Anna, CA) and Nanotechnologies, Inc. (Austin, TX).
5. D. E. G. JONES, R. TURCOTTE, Q. KWOK and M. VACHON, "Comparative Studies of the Thermal Hazards of Aluminum Nanopowders," in Proceedings from the 34th International Annual Conference of ICT (Institut Chemische Technologie, June 2003).
6. Q. S. M. KWOK, R. C. FOUCHARD, A.-M. TURCOTTE, P. D. LIGHTFOOT, R. BOWES, and D. E. G. JONES, "Characterization of Aluminum Nanopowder Compositions," Propellants, Explosives and Pyrotechnics, in press (2003).
7. J. J. GRANIER and M. L. PANTOYA, "Laser Ignition of Nanocomposite Thermites," To appear in *Combustion and Flame* 2004.
8. E. M. HUNT, K. B. PLANTIER and M. L. PANTOYA, *Acta Materialia* **52**(11) (2004) 3183.
9. J.-P. LEBRAT, A. VARMA and P. J. MCGINN, *J. Mater. Res.* **9**(5) (1994) 1184.
10. I. M. HUTCHINGS, *Powder Technology* **76** (1993) 3.
11. A. S. MUKASYAN, A. S. ROGACHEV and A. VARMA, *Chem. Engng. Sci.* **54** (1999) 3357.
12. A. S. DUBROVIN, L. V. SLEPOVA, and V. L. KUZNETSOV, *Comb. Explos. Shock Waves* (Engl. Transl.) **6** (1970) 60.
13. A. MAKINO and C. K. LAW, *J. Amer. Ceram. Soc.* **77**(3) (1994) 778.
14. R. TOMASI and Z. A. MUNIR, *ibid.* **82**(8) (1999) 1985.
15. R. ARMSTRONG, *Comb. Sci. and Techn.* **71** (1990) 155.
16. J. ECKERT, J. C. HOLZER, C. C. AHN, Z. FU and W. L. JOHNSON, *Nanostructu. Mater.* **2**(4) (1993) 407.
17. H. J. FENG, J. J. MOORE and D. G. WIRTH, "The Combustion Synthesis of TiB2-Al_2O_3-Al Composite Materials," Proceedings of the Symposium on Developments in Ceramic and Metal Matrix Composites, TMS Annual Meeting, TMS, San Diego (1992) p. 219.
18. J. J. MOORE, D. W. READEY, H. J. FENG, N. PERKINS and D. G. WIRTH, *Adv. Powder Metall., Part. Mater. Proc.* **9** (1992) 381.

Received 11 May
and accepted 13 May 2004